AGU PUBLICATIONS

JGR

Journal of Geophysical Research: Atmospheres

RESEARCH ARTICLE
10.1002/2016JD025143

Key Points:
- Pure XG particles activate as CCN consistent with kappa = 0.1
- CCN-derived kappa is about 40% higher compared to HTDMA derived kappa for xanthan gum salt mixtures at RH = 90%
- Polymer/salt cross-links may suppress hygroscopicity relative to the ZSR prediction at low water activity

Supporting Information:
- Supporting Information S1
- Datasets S1–S11

Correspondence to:
N. Meskhidze and M. D. Petters,
nmeskhidze@ncsu.edu;
markus_petters@ncsu.edu

Citation:
Dawson, K. W., M. D. Petters, N. Meskhidze, S. S. Petters, and S. M. Kreidenweis (2016), Hygroscopic growth and cloud droplet activation of xanthan gum as a proxy for marine hydrogels, *J. Geophys. Res. Atmos.*, *121*, 11,803–11,818, doi:10.1002/2016JD025143.

Received 25 MAR 2016
Accepted 20 SEP 2016
Accepted article online 23 SEP 2016
Published online 13 OCT 2016

Hygroscopic growth and cloud droplet activation of xanthan gum as a proxy for marine hydrogels

K. W. Dawson[1], M. D. Petters[1], N. Meskhidze[1], S. Suda Petters[1], and S. M. Kreidenweis[2]

[1]Department of Marine Earth and Atmospheric Sciences, North Carolina State University, Raleigh, North Carolina, USA, [2]Department of Atmospheric Science, Colorado State University, Fort Collins, Colorado, USA

Abstract Knowledge of the physical characteristics and chemical composition of marine organic aerosols is needed for the quantification of their effects on cloud microphysical processes and solar radiative transfer. Here we use xanthan gum (XG)—a bacterial biopolymer—as a proxy for marine hydrogels. Measurements were performed for pure XG particles and mixtures of XG with sodium chloride, calcium nitrate, and calcium carbonate. The aerosol hygroscopicity parameter (κ) is derived from hygroscopic growth factor measurements (κ_{gf}) at variable water activity (a_w) and from cloud condensation nuclei activation efficiency (κ_{ccn}). The Zdanovskii, Stokes, and Robinson (ZSR) hygroscopicity parameter derived for multicomponent systems ($\kappa_{mix,\,sol}$) is used to compare measurements of κ_{gf} and κ_{ccn}. Pure XG shows close agreement of κ_{gf} (at $a_w = 0.9$) and κ_{ccn} of 0.09 and 0.10, respectively. Adding salts to the system results in deviations of κ_{gf} (at $a_w = 0.9$) from κ_{ccn}. The measured κ_{gf} and ZSR-derived hygroscopicity parameter ($\kappa_{mix,\,sol}$) values for different solutions show close agreement at $a_w > 0.9$, while κ_{gf} is lower in comparison to $\kappa_{mix,\,sol}$ at $a_w < 0.9$. The differences between predicted $\kappa_{mix,\,sol}$ and measured κ_{gf} and κ_{ccn} values are explained by the effects of hydration and presence of salt ions on the structure of the polymer networks. Results from this study imply that at supersaturations of 0.1 and 0.5%, the presence of 30% sea salt by mass can reduce the activation diameter of pure primary marine organic aerosols from 257 to 156 nm and from 87 to 53 nm, respectively.

1. Introduction

Marine hydrogels are dilute systems comprising three-dimensional random anionic polymer networks dispersed in seawater. Polymer chains collide due to Brownian motion and form cross-linked globules that can reach several micrometers in size. Self-assembly and dispersion of globules are in thermodynamic equilibrium with the dissolved organic carbon pool [*Chin et al.*, 1998]. Gels concentrate nutrients and thus help to sustain the oceanic microbial loop [*Verdugo*, 2012]. Hydrogels at the air-water interface and in the ocean pelagic zone are colloidal aggregates [*Verdugo*, 2012] and can be a component of the sea-surface microlayer in surface films or in visible slicks concentrated by the action of capillary wave-damping [*Cunliffe et al.*, 2013]. Bubble bursting processes can inject some of this organic material into the atmosphere as marine primary organic matter, potentially influencing hygroscopic properties and cloud condensation nuclei (CCN) potential of sea spray aerosol [*Orellana et al.*, 2011; *Gantt and Meskhidze*, 2013].

Marine hydrogels have been postulated to be an important contributor to sea spray aerosol due to their unique physicochemical and hydrological properties [*Ovadnevaite et al.*, 2011]. Fundamentally, the stability of the network and observed globule volume in water depends on the strength of the polymer cross-links. The strength of the polymer cross-links is determined by the physical properties of the polymer (charge-density, hydrophobic/hydrophilic domain ratios, flexibility, topology, quaternary conformation, and the molecular size of the polymer chains), as well as the availability of high-valence cations that replace the bound hydronium molecule [*Verdugo*, 2012]. Small changes in pH, temperature, and availability of salts can often result in considerable changes to the gel network, influencing its hydration properties [*García-Ochoa et al.*, 2000; *Verdugo*, 2012].

Köhler theory [*Kohler*, 1936] predicts the relationship between dry diameter, chemical composition, and supersaturation (ss) required to activate particles composed of common constituents of the atmospheric aerosol, including acids, salts, and organic compounds [e.g., *Raymond and Pandis*, 2002, 2003; *Bilde and Svenningsson*, 2004; *Petters and Kreidenweis*, 2007; *Koehler et al.*, 2009; *Petters et al.*, 2009a; *Pöschl et al.*,

Table 1. Properties of Chemicals Used[a]

Compound	Formula	MW (kg mol^{-1})	ρ (g cm^{-3})	α (m^3 mol^{-1})	C (vol/vol)	ε (vol/vol)
XG[b]	$(C_{35}H_{49}O_{29})_n$	10^3 to 10^4	1.61 ± 0.22	1 to 10	soluble	1
Sodium chloride[c]	NaCl	0.058	2.17	2.67e^{-5}	0.17	0.04
Calcium carbonate[c]	$CaCO_3$	0.100	2.71	3.69e^{-5}	4.80e^{-6} [d]	0.06
Calcium nitrate	$Ca(NO_3)_2 + 4H_2O$	0.236	1.82	1.30e^{-4}	0.77[e]	0.18
	$Ca(NO_3)_2$	0.164	2.50[f]	6.56e^{-5}	0.58[e,f]	0.14[f]

[a]MW: molecular weight, ρ: density, α: molar volume, C: solubility in water, and ε: volume fraction of solute "i" to total solute.
[b]Xanthan gum has a molecular weight distribution depending on the association between chains and the degree of aggregation, which is in part controlled by the fermentation conditions [*García-Ochoa et al*., 2000]. The density of XG is unknown. Dextrans and pullulan, which have chemically similar polysaccharides, have densities ranging between 1.4 and 2.0 g cm^{-3} [*Eckelt et al*., 2008]. In this work, we measured $\rho = 1.61$ g cm^{-3} (supporting information) and assume $\alpha = 5$ m^3 mol^{-1} for calculations that explicitly depend on either ρ or α.
[c]Properties taken from *Haynes et al.* [2015], CRC Handbook of Chemistry and Physics.
[d]Taken from *Aylward and Findlay* [1999], SI Chemical Data Book 4th edition.
[e]Taken from *Sullivan et al*. [2009].
[f]Used in calculations for mixed hygroscopicity.

2010; *Suda et al*., 2014]. Hygroscopic components in the particle form an aqueous solution that is in equilibrium with the vapor field. The aerosol-phase water content is governed by the water activity of the solution and is modulated by the vapor pressure enhancement due to drop curvature. Köhler theory is based on Raoult's law, which does not apply to aqueous solutions of soluble macromolecules. Alternative theories for macromolecule-water interactions have been successfully applied to better predict water contents in single-component systems [*Mikhailov et al*., 2003; *Petters et al*., 2006]. However, it is not clear whether these treatments are applicable to the molecules that form hydrogels. Despite their potential importance as CCN in the atmosphere, the water uptake and CCN activation properties of marine hydrogel aerosol particles have neither been investigated experimentally nor explained from an appropriate theoretical basis.

In this study, we report measurements of hygroscopic growth and cloud droplet activation properties of pure and internally mixed xanthan gum (XG) aerosol as a model for marine hydrogel aerosol. XG is a bacterial polysaccharide biopolymer [*García-Ochoa et al*., 2000] with an acidic character that is used as a reference standard to quantify transparent exopolymer particles in the ocean [*Malpezzi et al*., 2013]. Due to its importance as a hydrogel in the food and pharmaceutical industries, its hydration properties have been extensively studied, providing a basis for interpretation of our measurements of hygroscopic growth and cloud droplet activation. To mimic likely mixtures in marine aerosol, the measurements were carried out for mixtures comprising XG and salts containing sodium and calcium cations, choices consistent with their prevalence in the bulk ocean water or in the self-assembling microgels found in the ambient marine environment [*Chin et al*., 1998; *Verdugo*, 2012]. Further information about XG, including the chemical structure, is provided in Figure S1 and Text S1 in the supporting information.

2. Materials and Methods

2.1. Solution Preparation

Pure and mixed solutions were prepared by using the following chemicals (Table 1): XG (Sigma Aldrich, ≥99.9% pure), sodium chloride, NaCl (Sigma Aldrich, ≥99.5% pure), calcium carbonate, $CaCO_3$ (ACROS Organics, 98% pure), calcium nitrate tetrahydrate, $Ca(NO_3)_2 + 4(H_2O)$ (Sigma Aldrich, ≥99.0% pure), ammonium sulfate, $(NH_4)_2SO_4$ (Sigma Aldrich, ≥99.9% pure), and ultrapure water with 18.2 MΩ cm^{-1} resistivity with less than 5 ppm of impurities. Four bulk solutions were used for aerosol generation in this study: pure XG and XG mixed with NaCl, $CaCO_3$, and $Ca(NO_3)_2$, with solution bulk compositions as shown in Table 2. Sodium chloride was used due to its prevalence in seawater and the ability to compare results of our study with other researchers who used the XG-Na^+ mixed system [e.g., *Yoshida et al*., 1992; *Wyatt and Liberatore*, 2009]. Calcium is used here following the study by *Chin et al*. [1998] who showed that self-assembling microgels found in the sea have an affinity for the uptake of Ca^{2+} rather than Mg^{2+} or K^+, all of which can be abundant in seawater. *Chin et al*. [1998] further reported that slight increases in pH of the polymer-salt matrix with

Table 2. Results From gf and CCN Experiments[a]

Solution	m_s (g/100 mL H_2O)	ss (%)	D_{act} (nm)	κ_{gf}	$\kappa_{mix,\ sol}$ ($\kappa_{mix,\ insol}$)	$\kappa_{ccn} \pm 1\sigma$	$\langle\kappa_{ccn} \pm 1\sigma\rangle$	$\kappa_{mix,ccn}$	κ_R
XG	0.1	0.46	89	0.09 ± 0.01 (n = 6)	0.08[b] (–)	0.10 ± 0.01 (n = 3)	0.10 ± 0.01	0.10	NA[e]
		0.69	67			0.10 (n = 3)			
		0.91	53			0.11 (n = 3)			
XG + NaCl	0.1 + 0.005	0.46	75	0.12 (n = 2)	0.13 (0.08)	0.15 ± 0.01 (n = 3)	0.16 ± 0.01	0.14	1.28[f]
		0.69	57			0.16 ± 0.01 (n = 3)			
XG + $Ca(NO_3)_2$	0.1 + 0.025	0.46	73	0.12 ± 0.01 (n = 3)	0.19 (0.07)	0.17 ± 0.01 (n = 3)	0.18 ± 0.01	0.20[c]	0.82[g]
		0.69	55			0.18 ± 0.01 (n = 3)			
		0.91	45			0.19 ± 0.01 (n = 3)			
XG + $CaCO_3$	$(12.0 + 1.3) \times 10^{-3}$	0.46	79	0.07 (n = 3)	0.14 (0.08)	0.13 ± 0.01 (n = 3)	0.14 ± 0.02	0.15 [d]	0.97[g]
		0.69	58			0.15 (n = 3)			
		0.91	51			0.13 ± 0.03 (n = 3)			

[a] m_s: mass of solute (XG + salt) dissolved in 100 mL H_2O, ss: supersaturation, D_{act}: diameter where 50% of the particles activated, κ_{gf} : hygroscopicity parameter for a_w = 0.9 derived from growth factor measurements via equation (1) with reported ±1 standard deviation (n = number of samples), $\kappa_{mix,\ sol(insol)}$: ZSR-calculated mixed hygroscopicity for a_w = 0.9 with considered solubility, κ_{ccn}: hygroscopicity parameter derived via equation (3) with reported ±1 standard deviation (n = number of samples), $\langle\kappa_{ccn} \pm 1\sigma\rangle$: mean of κ_{ccn} with the mean of the standard deviation for the prepared solutions, $\kappa_{mix,ccn}$: ZSR-calculated mixed hygroscopicity for unit solubility and CCN measurements, κ_R: intrinsic hygroscopicity parameter for select salts.
[b] The parameterized value for XG at a_w = 0.9.
[c] The density for $Ca(NO_3)_2$ used in this calculation is $\rho = 2.5\ g\ cm^{-3}$.
[d] If solubility is taken into account, this value reduces to 0.09 with $H(x_i) = 0.01$.
[e] Not available for organic polymers of unknown molecular weight and density.
[f] κ intrinsic for NaCl from *Petters and Kreidenweis* [2007].
[g] κ intrinsic for $CaCO_3$ and $Ca(NO_3)_2$ from *Sullivan et al.* [2009].

respect to the ocean (from 8.2 to 8.5–9) could result in mineralization of Ca^{2+} within the matrix. Therefore, $Ca(NO_3)_2$ was chosen to suppress the formation of precipitates in the aerosol phase.

For solution (1), XG was dissolved in 50°C water to ensure that no undissolved powder residues were present in the solution and all solutions were used within 10 days of their preparation. The side chains of the XG polymer can uptake ~2 ions of Na^+ or ~1 ion of Ca^{2+} per monomer [*Rosalam and England*, 2006]. Solution (2), the NaCl-containing solution, was kept at 0.1% wt/wt of XG mixed with 0.005% wt/wt of NaCl; i.e., NaCl represented 5% of XG mass (~3% volume). For solutions containing calcium, i.e., solutions (3) and (4), amounts of $CaCO_3$ and $Ca(NO_3)_2$ were added to achieve equimolar concentration of Ca^{2+} ions relative to the total number of carboxylic (COOH) groups in solution. For the third solution, the mixture of XG and $CaCO_3$, the XG concentration was adjusted to the solubility limit of $CaCO_3$, i.e., 0.012% wt/wt of XG for 0.0013% wt/wt of $CaCO_3$. All polymer-salt complexes were mixed such that no residual cations should have been left unbonded or salts undissolved. This is discussed further in section 3, and a quantitative explanation can be found in Text S1.2.

Particles were generated via spray atomization of bulk solutions by using a Collison-type atomizer (TSI Inc. model 3076). One caveat to our analysis is the characterization of the chemical composition of the atomized particles. Deviations of particle composition from prepared stock solutions have been suggested as a possibility when generating aerosol by using Collison atomizers with solutions containing insoluble species [*Creamean et al.*, 2014]. Deviations in aerosol composition from stock solutions may also arise from the presence of surface active compounds in Collison atomizers [*Petters and Petters*, 2016] and electrospray generation systems [*MacMillan et al.*, 2012]. It is therefore possible that the formation of colloidal aggregates or the surface activity of XG may lead to fractionation effects during particle generation. The methodology used in this study cannot resolve this effect, and it is therefore assumed that the particle composition equals that of the stock solution. An ammonium sulfate solution at 0.1% wt/wt was used for calibration.

2.2. Hygroscopicity Parameter Derived From Growth Factor Measurements

Figure 1 shows a schematic view of the Hygroscopicity Tandem Differential Mobility Analyzer (HTDMA) setup. The instrument is similar to a version described previously [*Suda and Petters*, 2013]. In brief, the instrument consists of two atomizers for particle generation, a Nafion drying system, two high-flow differential mobility analyzers (DMA), and a humidification system. The second DMA is actively temperature controlled and insulated to permit stable measurements up to 99% relative humidity (RH) [*Suda and Petters*, 2013].

Particle-free clean air was used to atomize the solutions. The liquid feed to the atomizer was achieved through the use of syringe pumps at a flow rate of 30 μL/min. Particles were alternately drawn into the setup

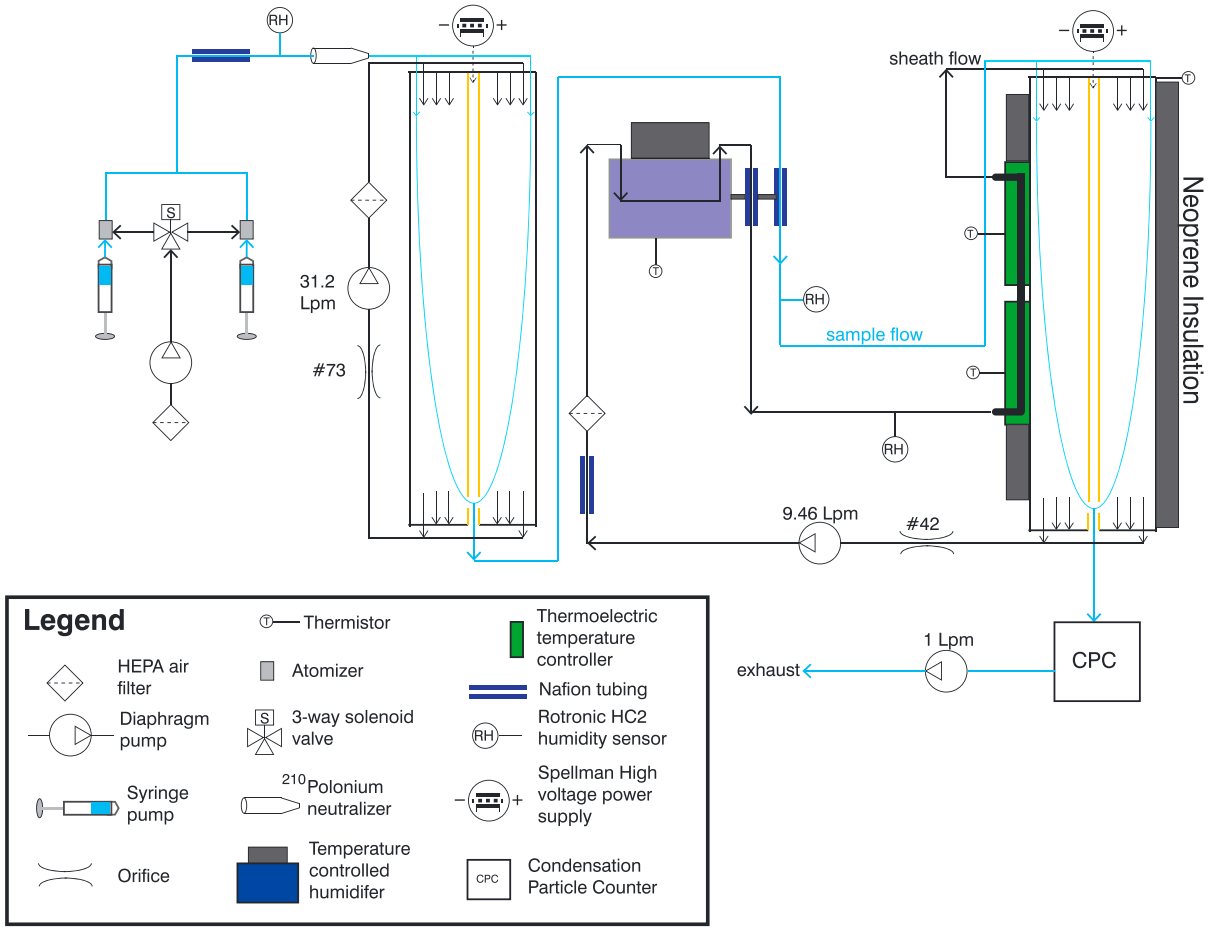

Figure 1. Schematic of the HTDMA setup.

by using one of two atomizers, one for the testing solution and one for the reference 0.1% wt/wt $(NH_4)_2SO_4$ solution. Generated particles were dried to relative humidity (RH) ~15% and charge equilibrated by using four ^{210}Po strips with a combined total activity of ~1 mCi before being passed to the first DMA. The first DMA was operated at a sheath to sample flow ratio of 27:1 Lpm and used to size select particles of nominal mobility diameter $D_{dry} = 100$ nm. The aerosol sample entering the second DMA was humidity controlled by passing sheath and sample air through a Nafion humidifier. Dry scans were run with the second DMA at RH < 30% (25 ± 5%). Relative humidity was monitored by three RH sensors along the sample and sheath paths for the humidified DMA and at the atomizer exit. The residence time between the exit of the humidifier and the entrance of the DMA was calculated to be ~6 s. Relative humidity inside the second DMA was calculated based on the dewpoint temperatures of the humidified flows and the average temperature of the three thermistors mounted to the outside of the column. Thermoelectric heat exchangers mounted to the second DMA minimized the standard deviation of the three temperatures to ±0.01°C evaluated over a 6 h measurement period, permitting control of stable RH values up to 98%. The humidified size distribution was measured by using the second DMA operated at sheath to sample flow ratio of 9:1 Lpm. A condensation particle counter (CPC) (TSI Inc. model 3772) was used to measure the particle concentration.

One major difference between the instrument operation here and that reported in *Suda and Petters* [2013] is the scanning strategy. Here the second DMA was operated in scanning mobility particle sizer mode [*Wang and Flagan*, 1990]. The duty cycle of a single size distribution scan was 30 s hold at 3000 V, and exponential downscan to 10 V over 180 s and a 30 s flush. Procedures used to map the time-varying electric field to mobility diameter followed standard DMA theory [*Knutson and Whitby*, 1975; *Wang and Flagan*,

1990] and are described in further detail for our system in *Nguyen et al*. [2014]. The resulting humidified size distribution was fitted to find the mode diameter from which the growth factor was determined. A detailed description of the data reduction procedures, including example raw data, corrections due to diameter offsets between the two DMAs, offsets due to particle shape subsequent to drying, the scan-varying humidity, and the humidity calibration using reference aerosol are provided in the supporting information.

Modal dry (D_{dry}) and wet (D) diameters were used to define the growth factor: $gf(RH) = D/D_{dry}$. The hygroscopicity parameter is calculated following *Petters and Kreidenweis* [2007]:

$$\kappa_{gf} = \frac{(gf^3 - 1)(1 - a_w)}{a_w} \tag{1}$$

where water activity is $a_w = 0.01 \times \mathrm{RH}(\%)/\exp\frac{A}{D}$; $A = 2.1$ nm and a constant temperature (298 K), water density, surface tension of water and, with no data to support otherwise, volume additivity are assumed [*Petters and Kreidenweis*, 2007].

The performance of the instrument was evaluated by using glucose test particles. The derived κ_{gf} was within ±10% of bulk measurements [*Miyajima et al*., 1983] (supporting information). The equilibrium water content (X, mass of water over mass of dry solute) was also calculated for comparison of our XG gf to various polymer gum mass gf from the literature. If volume additivity is assumed, the equilibrium water content can be translated from gf and is

$$X = \frac{\rho_0}{\rho}(gf^3 - 1), \tag{2}$$

where ρ is the density of XG and is ~1.61 ± 0.22 g cm^{-3} [*Assis et al*., 2010] (supporting information). The value of ρ_0 is for water and is 1 g cm^{-3}. The relative uncertainty of the gf measurement and the measured density for XG were added in quadrature to give an uncertainty in X of 17%.

2.3. Hygroscopicity Parameter Derived From CCN Measurements

CCN concentrations were measured by using a setup similar to that of *Christensen and Petters* [2012]. In brief, the system consists of a TSI long DMA column in scanning mobility mode with sample flow split to either a 1 Lpm TSI 3772 CPC or a 0.5 Lpm Droplet Measurement Technologies continuous-flow streamwise thermal gradient CCN counter [*Roberts and Nenes*, 2005; *Moore et al*., 2010]. Experiments were performed at four thermal gradients, $\Delta T = 4$, 8, 12, and 16°C. The corresponding supersaturations for these settings were obtained by determining the activation diameter of ammonium sulfate reference particles [*Rose et al*., 2008]. The underlying water activity versus composition values for ammonium sulfate were determined from the Extended-Aerosol Inorganic Model [*Clegg et al*., 1998; *Wexler and Clegg*, 2002]. Further details on the calibration procedures are described in *Christensen and Petters* [2012]. The activated fraction was determined from the ratio of the activated to total particle concentration. Next the activated fraction was inverted to correct for multiply charged particles [*Petters et al*., 2009a] and fit with a sigmoidal model [*Petters et al*., 2007; *Sullivan et al*., 2009; *Suda et al*., 2012]. The activation diameter was taken as the point where 50% activation had occurred. The difference between the instrument operation here and that reported in *Christensen and Petters* [2012] was the dry diameter scanning strategy, which was changed from stepping to scanning mode [*Petters and Petters*, 2016]. The scan duty cycle was 5 s hold at 4000 V, followed by 180 s exponential downscan to 10 V, followed by a 20 s flush. Calibration data, inversion procedures, and example activation curves are provided in the supporting information. The hygroscopicity parameter determined from measurements by using this system is calculated following [*Petters and Kreidenweis*, 2007, 2013]:

$$\kappa_{ccn} = \frac{4A^3\sigma_{s/a}^3(T)}{27D_{act}^3T^3\ln^2 S_c} \tag{3}$$

where D_{act} is the fitted activation diameter and S_c is the saturation ratio inside the instrument and A is a constant equal to ~8.7×10^{-6} K m^3 J^{-1}. All calculations determining κ_{ccn} from equation (3) were carried out using $T = 298$ K and surface tension of water, $\sigma = 0.072$ J m^{-2}, to be consistent with the definition of *Petters and Kreidenweis* [2007]. More on the selection for the surface tension value can be found in section 4 as well as in the supporting information. Measured κ_{ccn} for glucose test particles typically fell within $\kappa_{ccn} \pm 0.02$ of the expected $\kappa_{ccn,\ glucose} = 0.16$, suggesting that the precision of the scanning mobility CCN method was $\kappa_{ccn} \pm 13\%$.

2.4. Mixed Particle Hygroscopicity

For multicomponent systems that satisfy the conditions of the Zdanovskii, Stokes, and Robinson (ZSR) assumption [*Zdanovskii*, 1948; *Stokes and Robinson*, 1966], the hygroscopicity parameter of the mixture, κ_{mix}, can be estimated from the pure component κ_i [*Petters and Kreidenweis*, 2008]

$$\begin{aligned} \kappa_{mix} &= \textstyle\sum_i \varepsilon_i \kappa_i H(x_i) \\ x_i &= \left(gf^3 - 1\right) C_i / \varepsilon_i \\ H(x_i) &= \begin{cases} x_i & x_i < 1 \\ 1 & x_i \geq 1 \end{cases} \end{aligned} \tag{4}$$

where i denotes different components in the mixture, ε_i is volume fraction of solute, C_i is the solubility in water (vol/vol), and $H(x_i)$ is a function based on the solubility value (x_i) of the ith component. Volume fractions are calculated from the mass fraction of each solute with measured density of XG and the densities for NaCl, $CaCO_3$, and $Ca(NO_3)_2$. Densities were obtained from the CRC Handbook of Chemistry and Physics [*Haynes et al.*, 2015] and are listed in Table 1. Note that $Ca(NO_3)_2$ tetrahydrate was used to dissolve in the bulk solution, and its properties are listed in Table 1. However, current theory considers the pure components of each constituent and so properties of the anhydrous $Ca(NO_3)_2$, also shown in Table 1, were used in all calculations.

We calculate κ_{mix} for conditions both below ($\kappa_{mix,\ sol(insol)}$, where sol(insol) is soluble or insoluble) and above ($\kappa_{mix,\ ccn}$) water saturation. To compare $\kappa_{mix,\ ccn}$ to the hygroscopicity parameter derived from CCN measurements (i.e., conditions at or above water saturation), equation (4) is used with the measured value of κ_{ccn} for XG and pure component hygroscopicity derived using Raoult's law (κ_R; calculated from density and molecular weight) [*Petters et al.*, 2009b] for NaCl, $CaCO_3$, and $Ca(NO_3)_2$. The value of $H(x_i)$ is set to 1 for all $\kappa_{mix,\ ccn}$ calculations under these conditions. The $\kappa_{mix,\ ccn}$ values for different mixtures and κ_R values for different salts are summarized in Table 2.

Additionally, to compare $\kappa_{mix,\ sol(insol)}$ to the hygroscopicity parameter derived from gf measurements (i.e., conditions below water saturation), equation (4) is applied under the condition of $x_i < 1$, when all the components may not be fully dissolved. This could be particularly necessary for $CaCO_3$, which may exceed its solubility limit at low a_w resulting in insoluble precipitates within the aerosol particle. The κ value for XG at different water activities is parameterized by fitting a second-order polynomial to the measurements within a 95% confidence interval (CI) of $0.05 \leq \kappa_{gf} \leq 0.12$. Water activities for NaCl and $Ca(NO_3)_2$ solutions are calculated for different mass fractions of water by the web-based version of the Aerosol Inorganic-Organic Mixtures Functional groups Activity Coefficients (AIOMFAC) model [*Zuend et al.*, 2008, 2011; http://www.aiomfac.caltech.edu] and then converted to κ by using pure component density, which is summarized in the supporting information. The κ value for $CaCO_3$ was set to $\kappa_R = 0.97$ since AIOMFAC solutions for a_w are not available for $CaCO_3$. Figure S7 shows the calculated solubility for each mixture.

3. Results

Figure 2 and Table 2 summarize our experimentally measured (by HTDMA and CCN methods) and theoretically derived hygroscopicity parameters for all solutions. Observed activation diameters for pure XG particles at $0.46\% < ss < 0.91\%$ varied from 89 to 53 nm, respectively. The average "dry" RH during size selection in the second DMA was 26.4% and 31.6% for each of the pure XG experiments, and the highest RH accessed experimentally was 98.3% and 95.9%, respectively (supporting information). Growth factors for ~98 nm pure XG particles were ~1.2 at a_w ~0.9, corresponding to $\kappa_{gf} = 0.09$ at $a_w = 0.9$. The observed gf for XG ranged between 1.05 at RH ~ 65% to gf = 1.5 at RH = 98%. Figure 2 and Table 2 further show that the CCN activity of the pure XG-water system was well represented by $\kappa_{ccn} = 0.1 \pm 0.01$, just slightly larger than κ_{gf}. The standard deviation of κ_{ccn} was ±0.01 ($n = 9$), which is within the κ_{ccn} ±13% precision of the measurement. Overall, measured growth factors and κ_{gf} and κ_{ccn} for XG were within the range of $0 < \kappa < 0.3$ that has been observed for a number of organic species [*Petters et al.*, 2009b; *Suda et al.*, 2014], including fresh and aged laboratory-generated secondary organic aerosol [*Virkkula et al.*, 1999; *Baltensperger et al.*, 2005; *Prenni et al.*, 2007; *Massoli et al.*, 2010]. Pure XG particles thus exhibit activation behavior similar to other organic compounds, e.g., secondary organic aerosol from *Prenni et al.* [2007] and norpinic acid at ss = 0.3% from *Raymond and Pandis* [2002].

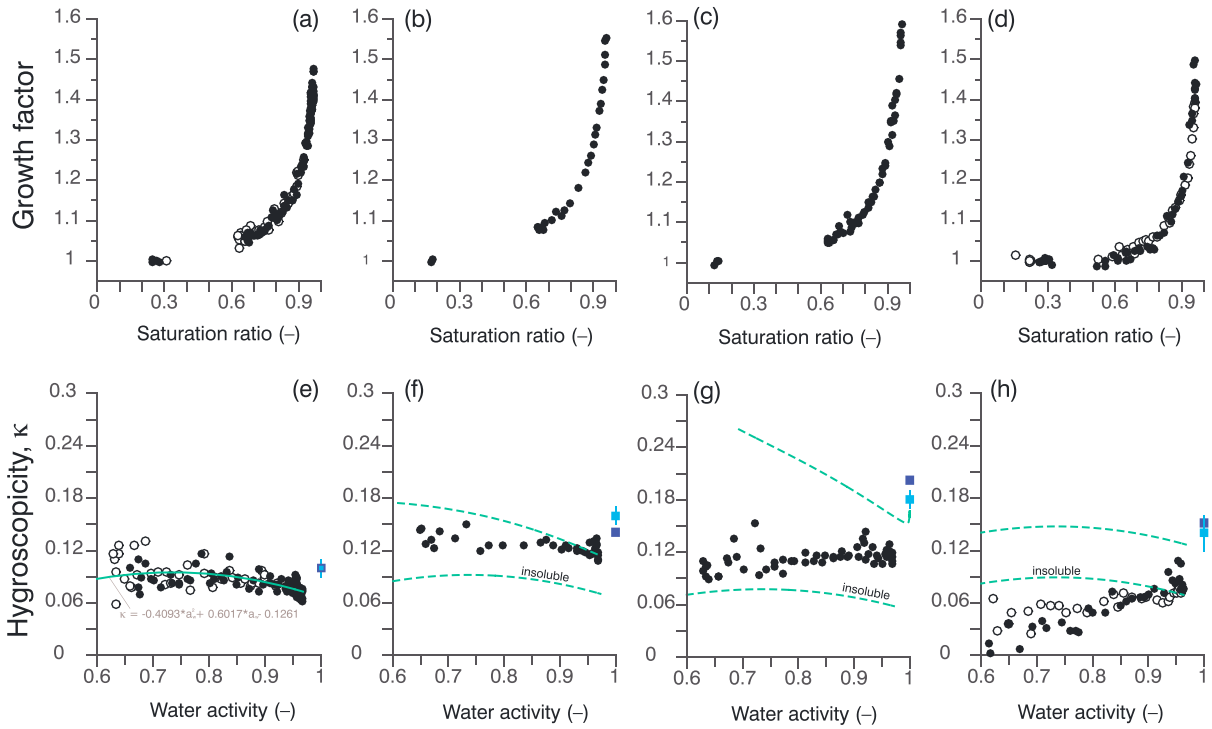

Figure 2. (top) Growth factors and (botttom) hygroscopicity parameters for the test solutions: (a and e) pure XG, (b and f) XG with NaCl, (c and g) XG with $Ca(NO_3)_2$, and (d and h) XG with $CaCO_3$. Two shades indicate experiments of the same composition solution repeated on different days (but no more than 10 days apart), and the light (dark) blue symbols on hygroscopicity plots show κ_{ccn} ($\kappa_{mix,\ ccn}$) with corresponding ±1 standard deviation. The solid green line in Figure 2e is a second-order fit of the XG data and used to compute κ_{mix} (dashed lines) for Figures 2f–2h considering $H(x_i)$ as in equation (4) (note that Figure 2f was fully soluble). The lower dashed green line is $\kappa_{mix,\ insol}$ assuming fully insoluble salts. Figures 2f and 2g use the AIOMFAC model for computing hygroscopicity of NaCl and $Ca(NO_3)_2$ for different a_w, and Figure 2h uses the intrinsic κ for $CaCO_3$ for calculating the upper dashed green line for $H(x_i) = 1$; these we refer to as $\kappa_{mix,\ sol}$. The 95% CI in the second-order fit including 10% measurement uncertainty is [0.05, 0.12]. The vertical green line in Figure 2g is the AIOMFAC model result,where $\kappa_{mix,\ sol}$ turns upwards at high water activity approaching κ_{ccn}. This does not happen for NaCl and $CaCO_3$ uses constant κ_R instead of AIOMFAC calculated, so the trend follows the XG parameterization in Figure 2e.

The addition of small amounts of salt, on the other hand, generally increased κ relative to pure XG, although κ remained lower than that for the pure salt. Table 2 and Figure 2f show that adding 5% of NaCl (dry mass fraction) increased the observed κ_{gf} by ~33% (0.12 at $a_w = 0.9$) and κ_{ccn} by ~60% (0.16 ± 0.01) with respect to pure XG. Addition of $Ca(NO_3)_2$ did not inhibit water uptake through the presence of insoluble components at $a_w > 0.67$ and measured hygroscopicity compared well to the κ_{gf} values of XG-NaCl mixtures (see Table 2 and Figure 2g). However, Table 2 and Figure 2h show that addition of $CaCO_3$ had a strong effect on the observed gf of XG particles. Figure 2h shows that at $a_w > 0.9$, measured κ_{gf} approached the pure XG value of 0.1, while at $a_w < 0.8$ there was a substantial inhibition of water uptake compared with pure XG, with κ_{gf} approaching zero (expected for insoluble material).

Figures 2f–2h also show the comparison of κ_{gf} of the mixed systems to $\kappa_{mix,\ sol(insol)}$ considering salt solubility limits (soluble(insoluble) for upper(lower) dashed green lines). The calculated $\kappa_{mix,\ sol}$ value for the mixture of XG with NaCl agrees closely (6% ± 5%) with the measurements at $a_w > 0.85$ (Figure 2f). However, deviation greater than the 10% measurement uncertainty between observed and calculated κ values can be seen for $a_w < 0.85$. Figure 2g shows that the observed κ for XG and $Ca(NO_3)_2$ mixtures is far from the ZSR calculated $\kappa_{mix,\ sol}$ (but perhaps approaching the limit of insoluble salt ($\kappa_{mix,\ insol}$) near $a_w = 0.6$) and the two values never reach agreement within the 10% measurement uncertainty. For the mixtures of XG with $CaCO_3$, κ_{mix} was calculated by (i) using measured solubility ($\kappa_{mix,\ insol}$ labeled as "insoluble" since $x_i \sim 0$) and (ii) with solubility prescribed as unity ($\kappa_{mix,\ sol}$, lines not labeled are for $H(x_i) = 1$). Figure 2h shows that $\kappa_{mix,\ sol}$ is closer to κ_{gf} when measured solubility is used in ZSR calculations at $a_w > 0.9$. Expectedly, there is little difference from parameterized XG in Figure 2e compared with $\kappa_{mix,\ insol}$ assuming insoluble salts in Figures 2f and 2g and $\kappa_{mix,\ insol}$

with calculated solubility for $CaCO_3$ in Figure 2h. This is explained by the minor reduction of $\kappa_{mix,\ insol}$ by the addition of small volume fractions of salt (Table 1).

Two main processes believed to play a role in the discrepancy between observed growth factor and ZSR-calculated $\kappa_{mix,\ sol}$ values are discussed next. First, the presence of insoluble material in aerosols cannot be ignored. Here we note that according to Figure 2h, it is clear that the assumption of complete solubility for $CaCO_3$ does not hold at all measured a_w. Our analysis based on observed gf, solute volume fraction, and solubility in water (see equation (4) and Figure S7) indicates the presence of insoluble components at the water content corresponding to conditions during hygroscopic growth and the critical wet diameter at CCN activation (see Table 2 footnotes). Second, the formation of physical cross-links between XG chains and salt cations is not accounted for by the thermodynamics of the ZSR mixing rules. Mainly, cross-linking between XG chains and salts violates the ZSR assumption that solute-solute interactions are negligible. It has been shown that Ca^{2+} and Na^{+} can bond with the polymer chains [*Ohmine and Tanaka*, 1982; *Verdugo*, 2012]. Then, depending on the resulting physical state, this bonding could contribute to deviation from the ZSR mixing rules as observed in the organic/inorganic mixtures by *Zardini et al*. [2008]. We prepared solutions such that the number of cations were approximately equimolar to the coordination sites on the XG chain (Figure S1 and Text S1.2). If each cation is fully bonded this would reduce the effective number of cations for the water to solvate, and thereby negate the influence of salt on increasing κ. Since the addition is approximately equimolar, a lower first-order estimate of the effect on κ would be the assumption that salt is effectively insoluble (see Figure 2). These pathways (insolubility and solute-solute interactions from cross-linking) for deviation from ZSR are not mutually independent and could operate synchronously.

In the context of our measurements, for XG with NaCl (Figure 2f) and XG with $Ca(NO^3)^2$ (Figure 2g), the observed κ_{gf} exceeds this lower limit, suggesting that the cations are not fully bonded and/or that the anions contribute to the hygroscopicity. A complete treatment of the problem will require accounting for the equilibrium between bound and unbound Na^{+} ions in solution. For XG with $CaCO^3$, the observed κ_{gf} is below the insoluble prediction, suggesting insoluble components. From our results follow two important distinctions. First, κ_{ccn} (i.e., hygroscopicity from CCN activation methods) will overestimate water uptake at subsaturated conditions (κ_{gf}) for these XG-salt complexes. Second, ZSR mixing rules ($\kappa_{mix,\ sol}$) for determining the hygroscopicity of XG-salt complexes at lower water content do not fully explain the observations here, especially those at $a_w < 0.9$.

4. Discussion

The following paragraphs discuss kinetic limitations, surface tension uncertainty, and physical interactions between XG molecules and different salts added to the system. Furthermore, results are presented in the framework of atmospheric and climatic relevance.

4.1. Salt Effects on Particle Microstructure

Figures 2f–2h and Table 2 show that closure (defined as agreement within ±10% measurement uncertainty) between κ_{ccn} and $\kappa_{mix,\ ccn}$ was achieved for solutions that did not contain insoluble material. Closure between κ_{gf} (for $a_w \geq 0.9$) and κ_{ccn} was also achieved for pure XG particles but not for the XG-salt mixed solutions. Closure between κ_{gf} and $\kappa_{mix,\ sol}$ was not achieved for any of the XG-salt mixed solutions at $a_w < 0.9$. The behavior of κ_{gf} and κ_{ccn}, relative to $\kappa_{mix,\ sol}$ at different a_w values and $\kappa_{mix,\ ccn}$ at $a_w \sim 1$, can perhaps be attributed to different hydration regimes of pure XG and XG-salt particles. Water-polymer mixtures exhibit distinct regimes in structure and properties that vary with the water content, ambient temperature, and presence of salts in solution [*Yoshida et al*., 1992; *Dobrynin et al*., 1995; *Wyatt and Liberatore*, 2009]. These regimes along with the entanglement behavior of the polymer gel structure are schematically shown in Figure 3 for an initially dry, 89 nm XG particle and will be used to interpret the observed differences between κ_{gf} and κ_{ccn}.

Upon contact of dry polymers with water molecules, polar hydrophilic groups are the first to be hydrated, which leads to the formation of nonfreezing or freezing bound water in highly concentrated solutions [*Yoshida et al*., 1992, 1998; *Hatakeyama et al*., 2012; *Tanaka et al*., 2013]. As the network swells, hydrophobic groups also capable of interacting with water molecules become exposed. In this concentrated regime, polymer chains remain entangled and rigid [*Wyatt and Liberatore*, 2009]. Under such conditions, water associated with the hydrogel exhibits physical properties different from that of free water. For example, this water could remain in the liquid state even at temperatures as low as −60°C [*Yoshida et al*., 1992; *Hatakeyama et al*., 2012;

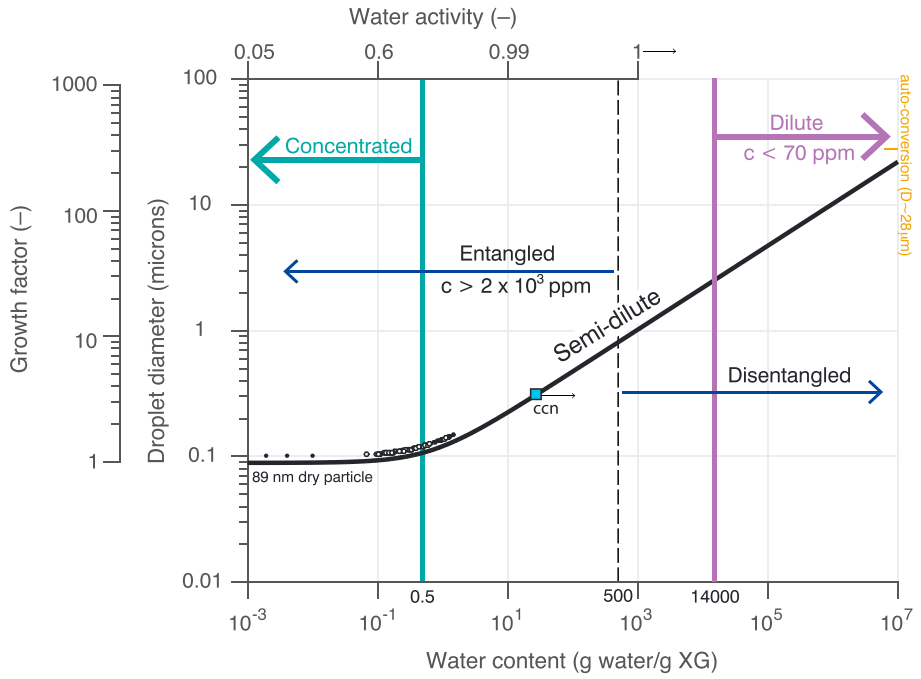

Figure 3. Regimes of behavior for the XG-water system as a function of water content (and water activity on the upper *x* axis). On the *y* axis, the water content is translated approximately into the hydrated diameter (neglecting the Kelvin effect) of an initially dry, 89 nm particle, assuming volumetric additivity of water and polymer and is shown by the black line using equation (3) (growth factor is also shown for reference). Surface tension for the XG-water system was assumed to be that of pure water. The XG concentrations (*c*) and corresponding water contents for dilute, semidilute, concentrated, entangled, and disentangled ranges were taken from *Yoshida et al.* [1992] and *Wyatt and Liberatore* [2009]. Growth factor and CCN (for D_{act} = 89 nm, ss = 0.46%) data for pure XG are overlaid as black outlined circles and a blue square, respectively.

Tanaka et al., 2013]. Further hydration (~0.5 g water/g XG) will move the system to the semidilute regime [*Yoshida et al.*, 1992]. Based on the polymer type and concentration, polymer chains can be entangled in the semidilute regime where water interacts weakly with the polymer chains [*Wisniewski and Kim*, 1980; *Tanaka et al.*, 2013] or disentangled in an elastic, liquid-like state with disordered conformation that can be physically described as a broken or imperfect helix [*Wyatt and Liberatore*, 2009]. Although the exact point of transition for XG is not well known, the approximate boundary for the change from an entangled to disentangled state is expected to occur at a polymer concentration of ~2000 ppm (500 g water/g XG) [*Wyatt and Liberatore*, 2009]. The additional absorbed water at concentrations <70 ppm (~1.4×10^4 g water/g XG) is assumed to fill the space between the network chains, and/or the center of larger pores, macropores, or voids and behave as "free water" or "bulk water" [*Gulrez et al.*, 2011].

While the exact mechanism for measured differences between κ_{gf}, $\kappa_{mix,\ sol}$, and κ_{ccn} for XG hydrogels cannot be ascertained based on this study, we believe that it is associated with the differences in the structure of the polymer networks due to water properties at different polymer concentrations. The schematic in Figure 3 shows that the hygroscopicity measurements for this study cover the range from the concentrated to the semidilute regime. Hygroscopicity measurements using the CCN technique are carried out toward the more dilute regions where polymer macromolecules are more separated from each other. Hygroscopicity measurements using the growth factor technique are primarily in a concentrated region where the cross-links between the entangled polymer chains are strong, especially in the presence of salt ions. This is further supported by the measured differences between κ_{gf}, $\kappa_{mix,\ sol}$, and κ_{ccn} for the pure XG + salt solutions, which showed pronounced deviation from the ZSR mixing rule at low a_w, an indication that the ZSR assumption of no interaction between mixture components for high molecular weight polymer + salt particles may break [*Zdanovskii*, 1948; *Stokes and Robinson*, 1966; *Zardini et al.*, 2008].

The presence of salt ions at the concentrations typically found in seawater can affect cross-links between XG hydrogel macromolecules, influence their rheological properties [*Wyatt and Liberatore*, 2009], and by

association their hygroscopicity. Monovalent salt cations like Na^+ and K^+ cause stabilization of xanthan chains in the helical conformation causing entanglement of the polymer chain structure compared to the extended highly disordered salt-free case [*Wyatt and Liberatore*, 2009]. Addition of NaCl to the XG-water system shifts the transition between concentrated and dilute regimes to higher solute concentrations (i.e., lower water contents) [*Wyatt and Liberatore*, 2009]. Figure 2f shows that, as expected, the presence of NaCl increases κ_{gf} at all water activity values compared to pure XG but is still less hygroscopic than the prediction from ZSR mixing (green dashed line in Figure 2f). Compared to a salt free solution, measured values of κ_{ccn} are higher and, according to Table 2, well represented by the ZSR mixing rule.

Divalent cations such as Ca^{2+} and Mg^{2+} tend to also affect physical cross-linking of the XG chain. However, unlike monovalent salt ions, Ca^{2+} ions can initiate crystallization and precipitation of gel-Ca complexes, particularly under alkaline conditions [*Chin et al*., 1998; *Verdugo*, 2012]. For water activity >0.9 both the XG-$CaCO_3$ (see Figure 2h) and the XG-$Ca(NO_3)_2$ (see Figure 2g) solutions show κ_{gf} values near or larger than that of the pure XG-water system. However, Figure 2h reveals suppression of κ_{gf} at water activity <0.9, possibly due to precipitation of XG-Ca^{2+} complexes. Interestingly, there is close agreement between κ_{ccn} and $\kappa_{mix,\ ccn}$ when we assume full solubility for the $CaCO_3$ solution, and for the semidilute regime (i.e., $a_w > 0.9$) the hygroscopicity of XG-Ca^{2+} mixtures approaches $\kappa_{mix,\ ccn}$ (see Table 2 and Figure 2). A possible explanation could be that XG-Ca^{2+} bonds prevent crystallization of the salt resulting in enhanced dissolution, which allows the system to fully express the prediction for $\kappa_{mix,\ ccn}$. Overall, results of our study suggest that there can be large differences between measured κ_{gf} and κ_{ccn} and ZSR calculated $\kappa_{mix,\ sol}$ values for hydrogels, especially in the presence of divalent salts. Future studies should be conducted to explore detailed mechanisms for the water uptake by hydrogels under different conditions characteristic of ambient aerosols.

4.2. Kinetic Limitations

The modeled characteristic time scale for 100 nm dry particles to equilibrate with the water vapor field for a step change in *RH* is <200 ms [*Snider and Petters*, 2008], much smaller than the 6 s transit time between the exit of the humidification region and the entrance of the second DMA or the ~30 s in the CCN column. However, kinetic limitations for droplet growth have been hypothesized for organics [*Chuang et al*., 1997] and observed for a mixture of ammonium sulfate and humic acid sodium salt at RH = 85% on time scales exceeding 10 s [*Sjogren et al*., 2007]. When equilibration was allowed for residence time scales between 4 and 40 s, *Sjogren et al*. [2007] reported a gf change from 1.12 to 1.16. The characteristic mixing time scale between the particle and the vapor depends on the particle diameter, diffusivity, and viscosity [*Zhang et al*., 2015]. To our knowledge there are no reported values for an equilibration time scale of water soluble macromolecules in the context of HTDMA measurements. However, equilibration time scales for a particle of a given diameter can be derived if the viscosity of a particle is known [*Zhang et al*., 2015, equation (4)]. *Wyatt and Liberatore* [2009] and *Renbaum-Wolff et al*. [2013] have reported values for viscosity of pure XG and secondary organic material, respectively. The highest concentration measured in *Wyatt and Liberatore* [2009] corresponded to a water content of ~165 g water/g XG and a viscosity of 6000 Pa s leading to a mixing time scale on the order of 1 s. However, our measurements were made for much lower water content and so we expect viscosity and mixing time to increase above this value. Extrapolating the measurements from *Wyatt and Liberatore* [2009] (using a constant log-log slope of 3.75) to our measured value of 0.27 g water/g XG (for the gf measurements at *RH* = 80%) yields a viscosity on the order of 10^{13} Pa s and mixing time of 10^{11} s for 100 nm particles, which is characteristic of a glassy, solid-like phase [*Renbaum-Wolff et al*., 2013]. Although we cannot directly evaluate the role of kinetic limitations for equilibration time in our measurements, the above discussion suggests that viscosity might have caused deviation from equilibrium, especially at lower water activity. Figure 4 compares the observed water content from HTDMA results to equilibrium sorption isotherm data from *Basu et al*. [2007] and *Torres et al*. [2012]. Figure 4 emphasizes two points. First, our XG results are within the range of equilibrium water content for various gums, thus providing some context on the role of uncertainties due to kinetic limitations on expected growth for similar polysaccharides. Second, the water contents of these hydrogels appear predictable and, comparing the XG results that indicate a κ ~0.1, are not unusually large compared with other aerosols, even organics. The difference between our results and those shown in Figure 4 could also be attributed to the measurement uncertainties in XG density. Until XG density is better quantified, the shown error boundaries of ±17% are most likely a conservative estimate. Nonetheless, the comparison of our results with equilibrated XG water contents from *Basu et al*.

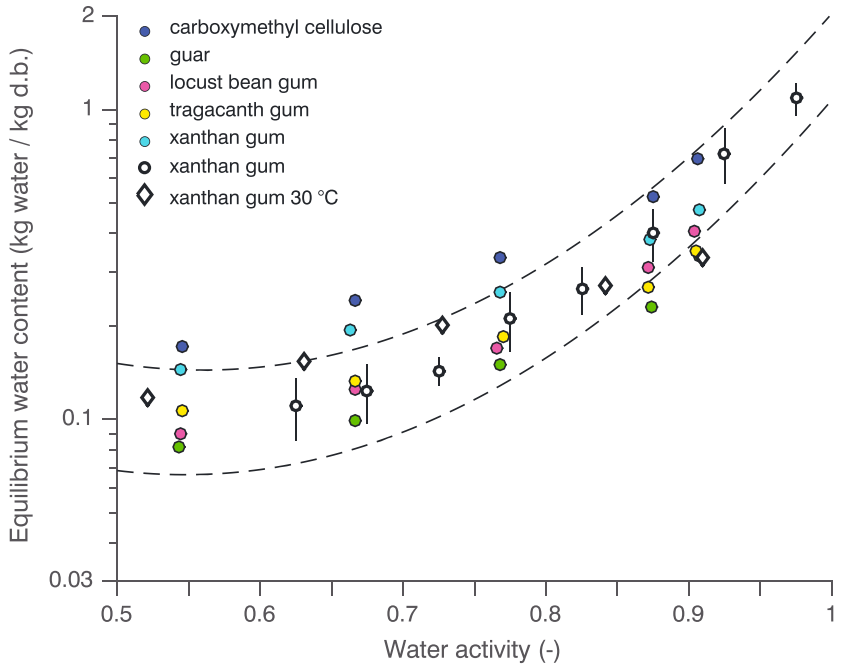

Figure 4. Pure XG equilibrium water content (translated from gf as in equation (2)) along with other organics observed by *Torres et al*. [2012] for 20°C (colored points) and *Basu et al*. [2007] (black diamonds) for 30°C. The open circles show XG data from Figure 2a but binned in 0.05 a_w intervals. The vertical bars indicate ±1 standard deviation within our binned data. The dashed black lines show ±17% uncertainty (added in quadrature), which considers both the ±10% uncertainty in the measurement as well as the ±0.22 g cm^{-3} standard deviation in the XG density used.

[2007] and *Torres et al*. [2012] suggests that kinetic limitations for the diffusion of water vapor into pure XG particles did not play a substantial role during our experiment.

4.3. Surface Tension

Organic components can lower the surface tension of the particle at the solution/air interface. *Lee et al*. [2012] measured the surface tension of XG for various concentrations. Measurements from *Lee et al*. [2012, and references therein] yield a lower limit for XG surface tension equal to 0.042 J m^{-2} at concentrations of ≥1% vol/vol (supporting information). Based on the observed κ_{gf}, we estimate that CCN activation for sizes and supersaturations encountered in this study proceeds at ~2% vol/vol. Based on bulk data, one would expect that the surface tension is 0.042 J m^{-2} or less, which is significantly lower than the value of pure water. However, estimates of the effect of reduced surface tension on CCN activity are inconsistent with those obtained from bulk surface tension measurements and classical Köhler theory [*Sorjamaa et al*., 2004; *Petters and Kreidenweis*, 2013; *Petters and Petters*, 2016]. At the molecular level surfactants migrate to the water/air interface, which sets up a radial concentration gradient within the aqueous droplet. Conceptually, the drop can be envisioned as a two-phase solution comprising a surface phase and bulk phase. Calculating the effect of surfactants on water uptake and CCN activity requires accurate prediction of the solute concentration in both phases. While thermodynamic models including this effect have yielded broad agreement with observations [*Sorjamaa et al*., 2004; *Petters and Kreidenweis*, 2013], full closure between observed bulk surface tension and observed κ_{ccn} is not always achieved by using these models, even for particles composed of well-characterized water soluble surfactants [*Petters and Petters*, 2016]. One fundamental limitation in validating the thermodynamic models is the inability to experimentally confirm the solute concentration in the surface and bulk phase, as well as measurement of the actual surface tension in the microscopic droplet.

For XG aerosol, modeling of the composition of the surface and bulk phase is further complicated by two effects. *Petters and Kreidenweis* [2013] suggested that kinetic limitations may prevent the formation of the surface phase at the time scale of CCN experiments where the high viscosity of XG solutions may limit the free exchange of molecules between the bulk and surface phase. It is therefore possible that viscosity prevents

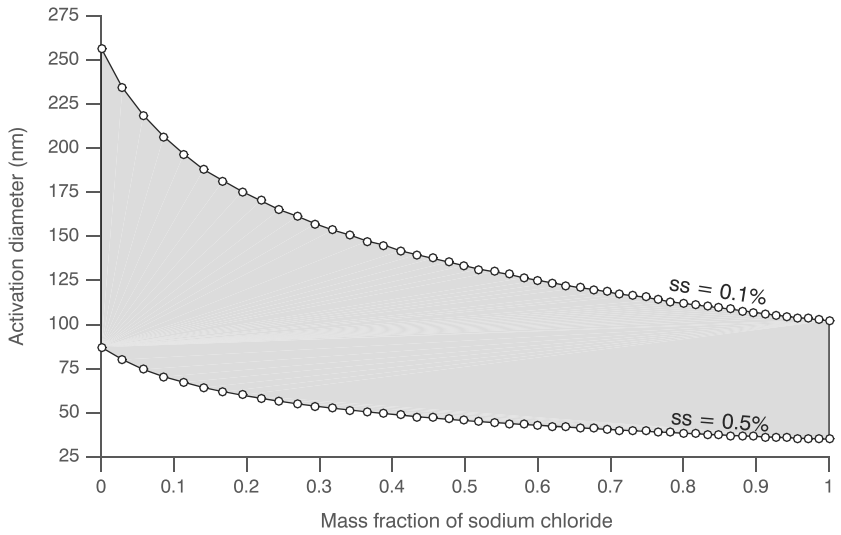

Figure 5. CCN activation diameter for XG-NaCl particles with a solute mass fraction of NaCl from 0 to 1 for two different values of ss typical for the marine environment (see text for references).

the formation of the radial surfactant gradient inside the droplet. Second, estimates of solute activity in basic partitioning theory are based on Raoult's law, e.g., the formulation of *Petters and Kreidenweis* [2013] based on the analytical approximation of *Raatikainen and Laaksonen* [2011]. However, as discussed above, Raoult's law breaks down for macromolecules, essentially predicting zero activity for MW ~ 10^7 g mol^{-1} [*Petters et al*., 2006]. Therefore, the standard approach would need revision to become applicable for XG aerosol. Unresolved questions about the accuracy of the existing theoretical frameworks [*Petters and Petters*, 2016], together with the added uncertainty of the roles of viscosity and applicability of Raoult's law, will require additional studies before the effect of surface tension on the observed κ_{ccn} for XG particles can be determined.

4.4. Atmospheric Implications

The XG-salt particles used in this study were selected to mimic the composition and size of submicron sea spray aerosols produced through bursting bubbles from ocean breaking waves. Our results show that pure organic aerosols produced from XG should activate at ~257 nm and ~87 nm dry diameter in shallow marine clouds at ss of 0.1 and 0.5%, respectively (see Figure 5). Considering that the hygroscopicity parameter reflects a particle's chemical composition and is theoretically size-independent, results of our study suggest that addition of marine hydrogels (which are less hygroscopic than sea salt) should lower CCN activity of sea spray particles. This result is consistent with both a water tank experiment performed in natural seawater using three different particle generation techniques (i.e., sintered glass filters, a pulsed-plunging waterfall, and continuous wave breaking) [*Prather et al*., 2013] and for laboratory produced marine aerosol using a plunging-water jet system of organically enriched seawater [*Fuentes et al*., 2010]. *Ovadnevaite et al*. [2011] observed CCN activation efficiency between 83% (at ss = 0.25%) and 100% (at ss > 0.75%) for predominately hydrophobic (gf = 1.25 at 90% RH, κ_{gf} = 0.12 for 100 nm dry particles) ambient marine aerosol with enrichment of 60–70% primary organic matter.

Figure 5 shows different activation diameters calculated from $\kappa_{mix,\ ccn}$ for different mass fractions of XG and NaCl. The steepest slopes for activation diameter versus mass fraction curves occur at low ss and mass fraction (mf) of NaCl. For example, compared to pure XG particles, addition of 30% NaCl at 0.1% ss lowers the activation diameter by ~100 nm. Continued increase in NaCl from mf = 0.3 to mf = 0.7 (or viewed as a decrease in organic content from mf = 0.7 to mf = 0.3) only lowers the activation diameter by another ~10 nm. The larger reduction of activation diameter when small amounts of salts are added to the system (and conversely, the relative insensitivity of the addition of small amounts of organics to predominantly salt particles) can have important implications for CCN properties of submicron sea spray aerosol enriched in marine organic matter. Organic mass fraction can be up to 90% for sub-200 nm (aerodynamic diameter) sized sea spray aerosols [*O'Dowd et al*., 2008; *Russell et al*., 2010; *Ovadnevaite et al*., 2011; *Prather et al*., 2013]. According

to Figure 5, activation of aerosol mimics of sea spray enriched in marine organics for sizes that are climatically relevant (50 to 150 nm dry diameter) is very sensitive to sodium content (fully detailed ss versus dry diameter plot with overlaid κ for varying mf of NaCl can be found in Figure S6). Taking activation diameter reported in Figure 5 and assuming that components are added volumetrically, the "equivalent" diameter of NaCl for a XG-NaCl particle with mf = 0.3 is 90 nm at ss = 0.1% and 31 nm at ss = 0.5%. These sizes translate to an equivalent mass of 8×10^{-22} g and 3×10^{-23} g at the respective *ss*. Therefore, detection of single particle salt contents in the range of 10^{-23} to 10^{-22} g is crucial for an accurate assessment of marine organic matter-enriched sea spray aerosol activation properties for the conditions of the marine environment.

A wave tank experiment of *Collins et al*. [2013] reported 86 ± 5% reduction in CCN-derived hygroscopicity of freshly emitted sea spray aerosol following an increase in heterotrophic bacteria in seawater. Despite very little change in organic mass fraction (less than 15% increase throughout the experiment), a link between increased number of submicron insoluble organic matter and the lowering of hygroscopicity based on aerosol CCN activity was reported [*Collins et al*., 2013; *Prather et al*., 2013]. The results presented in this work further the discussion about the interaction of water-soluble polymer-salt complexes and sea salt both at subsaturated and supersaturated conditions.

5. Conclusions

In this study we have quantified hygroscopic properties of particles containing pure XG and XG mixed with NaCl, $CaCO_3$, and $Ca(NO_3)_2$. Results suggest good agreement between CCN derived (κ_{ccn}) and ZSR calculated κ_{mix} values. This result shows that hygroscopicity of marine hydrogels and its different mixtures can be predicted with known volume fractions of the solutes in supersaturated conditions. Our measurements also show that κ_{gf} derived at water activity (a_w) > 0.9 and κ_{ccn} agree within experimental error (±10%) only for pure XG particles but not for the XG-salt mixed solutions. The addition of small amounts of Ca^{2+} and Na^+ salts generally increased κ relative to pure XG with the exception of $CaCO_3$, which showed a strong decrease of κ at low water activity. Additionally, our measurements show that closure between growth-factor derived (κ_{gf}) and ZSR κ was not achieved for any of the XG-salt mixed solutions at $a_w < 0.9$ and was often larger than ±10%. These measurement differences were suggested to be a result of different regimes found during the hydration of pure XG and XG-salt particles, among other uncertainties surrounding viscosity and surface tension of the solution to air interface. This study showed that across a wide range of water activity, hygroscopicity of XG-salt particles is complex and is not currently well explained by the ZSR volume mixing rules at subsaturated conditions, especially at $a_w < 0.9$. Future studies should be conducted to fully examine hydration behavior, morphology, and viscous properties of XG (and hydrogels in general) under a variety of environmental conditions (e.g., temperature, RH, and acidity) and presence of salt ions at different concentrations.

This study also examined the effect of small amounts of salt mass on CCN activity of aerosols. Our calculations indicated that for supersaturations ranging from 0.1 to 0.5%, the addition of 30% NaCl by mass can decrease dry activation diameter of primary marine organic aerosols from 256 to 155 nm and from 87 to 53 nm, respectively. These dry diameter ranges have been shown to be climatically relevant sizes for emitted sea spray particles [*de Leeuw et al*., 2011]. Converting these size ranges to mass thus implies that sea-salt amounts as low as 10^{-23} g per particle can play an important role in the conditions under which aerosols activate as CCN. Therefore, future studies should pay particular attention to the detection of salt contents at these low concentrations.

Acknowledgments

This research was supported by the National Science Foundation through the grant AGS-1249273 and NASA grant NNX14AL89G. M.D.P., S.S.P., and S.M.K. acknowledge additional funding from the Department of Energy, Office of Biological and Environmental Sciences under grant DE-SC0010470. Supporting information is available and describes measurement methods and data processing. All xanthan gum relative humidity and growth factor data are made available as part of the supporting information. We also thank the helpful recommendations from Editor Lynn Russell and three anonymous reviewers.

References

Assis, T. F., E. E. G. Rojas, G. C. Guimarães, M. C. Coelho, A. V. Ramos, B. S. Costa, and J. S. R. Coimbra (2010), Kinematic viscosity and density of binary and ternary mixtures containing hydrocolloids, sodium chloride, and water, *Int. J. Thermophys.*, *31*(3), 513–524, doi:10.1007/s10765-010-0747-3.

Aylward, G., and T. Findlay (1999), *SI Chemical Data Book*, 4th ed., John Wiley, New York.

Baltensperger, U., et al. (2005), Secondary organic aerosols from anthropogenic and biogenic precursors, *Faraday Discuss.*, *130*, 265–278, doi:10.1039/b417367h.

Basu, S., U. S. Shivhare, and A. S. Mujumdar (2007), Moisture adsorption isotherms and glass transition temperature of xanthan gum, *Drying Technol.*, *25*(9), 1581–1586, doi:10.1080/07373930701539795.

Bilde, M., and B. Svenningsson (2004), CCN activation of slightly soluble organics: The importance of small amounts of inorganic salt and particle phase, *Tellus, Ser. B*, *56*(2), 128–134, doi:10.1111/j.1600-0889.2004.00090.x.

Chin, W. C., M. V. Orellana, and P. Verdugo (1998), Spontaneous assembly of marine dissolved organic matter into polymer gels, *Nature*, *391*(6667), 568–572, doi:10.1038/35345.

Christensen, S. I., and M. D. Petters (2012), The role of temperature in cloud droplet activation, *J. Phys. Chem. A*, *116*(39), 9706–9717, doi:10.1021/jp3064454.
Chuang, P. Y., R. J. Charlson, and J. H. Seinfeld (1997), Kinetic limitations on droplet formation in clouds, *Nature*, *390*(6660), 594–596, doi:10.1038/37576.
Clegg, S. L., P. Brimblecombe, and A. S. Wexler (1998), Thermodynamic model of the system $H^+ - NH_4^+ - SO_4^{2-} - NO_3^- - H_2O$ at tropospheric temperatures, *J. Phys. Chem. A*, *102*(12), 2137–2154, doi:10.1021/jp973042r.
Collins, D. B., et al. (2013), Impact of marine biogeochemistry on the chemical mixing state and cloud forming ability of nascent sea spray aerosol, *J. Geophys. Res. Atmos.*, *118*, 8553–8565, doi:10.1002/jgrd.50598.
Creamean, J. M., C. Lee, T. C. Hill, A. P. Ault, P. J. DeMott, A. B. White, F. M. Ralph, and K. A. Prather (2014), Chemical properties of insoluble precipitation residue particles, *J. Aerosol Sci.*, *76*, 13–27, doi:10.1016/j.jaerosci.2014.05.005.
Cunliffe, M., A. Engel, S. Frka, B. Gašparović, C. Guitart, J. C. Murrell, M. Salter, C. Stolle, R. Upstill-Goddard, and O. Wurl (2013), Sea surface microlayers: A unified physicochemical and biological perspective of the air–ocean interface, *Prog. Oceanogr.*, *109*, 104–116, doi:10.1016/j.pocean.2012.08.004.
de Leeuw, G., E. L. Andreas, M. D. Anguelova, C. W. Fairall, E. R. Lewis, C. O'Dowd, M. Schulz, and S. E. Schwartz (2011), Production flux of sea spray aerosol, *Rev. Geophys.*, *49*, RG2001, doi:10.1029/2010RG000349.
Dobrynin, A. V., R. H. Colby, and M. Rubinstein (1995), Scaling theory of polyelectrolyte solutions, *Macromolecules*, *28*(6), 1859–1871, doi:10.1021/ma00110a021.
Eckelt, J., R. Sugaya, and B. A. Wolf (2008), Pullulan and dextran: Uncommon composition dependent Flory-Huggins interaction parameters of their aqueous solutions, *Biomacromolecules*, *9*(6), 1691–1697, doi:10.1021/bm800217y.
Fuentes, E., H. Coe, D. Green, G. De Leeuw, and G. McFiggans (2010), On the impacts of phytoplankton-derived organic matter on the properties of the primary marine aerosol. Part 1: Source fluxes, *Atmos. Chem. Phys.*, *10*(19), 9295–9317, doi:10.5194/acp-10-9295-2010.
Gantt, B., and N. Meskhidze (2013), The physical and chemical characteristics of marine primary organic aerosol: A review, *Atmos. Chem. Phys.*, *13*(8), 3979–3996, doi:10.5194/acp-13-3979-2013.
García-Ochoa, F., V. E. Santos, J. A. Casas, and E. Gómez (2000), Xanthan gum: Production, recovery, and properties, *Biotechnol. Adv.*, *18*(7), 549–579, doi:10.1016/S0734-9750(00)00050-1.
Gulrez, S., G. Phillips, and S. Al-Assaf (2011), Hydrogels: Methods of preparation, characterisation and applications, in *Progress in Molecular and Environmental Bioengineering—From Analysis and Modeling to Technology Applications*, edited by A. Carpi, pp. 117–150, InTech, Croatia.
Hatakeyama, T., M. Tanaka, and H. Hatakeyama (2012), Thermal properties of freezing bound water restrained by polysaccharides, *J. Biomater. Sci., Polym. Ed.*, *21*(14), 1865–1875, doi:10.1163/092050610X486946.
Haynes, W. M., D. R. Lide, and T. J. Bruno (2015), *CRC Handbook of Chemistry and Physics*, 96th ed., edited by W. M. Haynes, CRC Press, Boca Raton, Fla.
Knutson, E. O., and K. T. Whitby (1975), Aerosol classification by electric mobility: Apparatus, theory, and applications, *J. Aerosol Sci.*, *6*(6), 443–451, doi:10.1016/0021-8502(75)90060-9.
Koehler, K. A., S. M. Kreidenweis, P. J. DeMott, M. D. Petters, A. J. Prenni, and C. M. Carrico (2009), Hygroscopicity and cloud droplet activation of mineral dust aerosol, *Geophys. Res. Lett.*, *36*, L08805, doi:10.1029/2009GL037348.
Kohler, H. (1936), The nucleus in and the growth of hygroscopic droplets, *Trans. Faraday Soc.*, *32*(2), 1152–1161, doi:10.1039/tf9363201152.
Lee, B. B., E. S. Chan, P. Ravindra, and T. A. Khan (2012), Surface tension of viscous biopolymer solutions measured using the du Nouy ring method and the drop weight methods, *Polym. Bull.*, *69*(4), 471–489, doi:10.1007/s00289-012-0782-2.
MacMillan, A. C., J. B. Morrison, C. W. Harmon, and S. A. Nizkorodov (2012), Enhancement of surfactants in nanoparticles produced by an electrospray aerosol generator, *Aerosol Sci. Technol.*, *46*(11), 1239–1245, doi:10.1080/02786826.2012.708946.
Malpezzi, M. A., L. P. Sanford, and B. C. Crump (2013), Abundance and distribution of transparent exopolymer particles in the estuarine turbidity maximum of Chesapeake Bay, *Mar. Ecol. Prog. Ser.*, *486*, 23–35, doi:10.3354/meps10362.
Massoli, P., et al. (2010), Relationship between aerosol oxidation level and hygroscopic properties of laboratory generated secondary organic aerosol (SOA) particles, *Geophys. Res. Lett.*, *37*, L24801, doi:10.1029/2010GL045258.
Mikhailov, E., S. Vlasenko, R. Niessner, and U. Pöschl (2003), Interaction of aerosol particles composed of protein and salts with water vapor: Hygroscopic growth and microstructural rearrangement, *Atmos. Chem. Phys. Discuss.*, *3*(5), 4755–4832, doi:10.5194/acpd-3-4755-2003.
Miyajima, K., M. Sawada, and M. Nakagaki (1983), Studies on aqueous solutions of saccharides. I. Activity coefficients of monosaccharides in aqueous solutions at 25.DEG.C, *Bull. Chem. Soc. Jpn.*, *56*(6), 1620–1623, doi:10.1246/bcsj.56.1620.
Moore, R. H., A. Nenes, and J. Medina (2010), Scanning mobility CCN analysis—A method for fast measurements of size-resolved CCN distributions and activation kinetics, *Aerosol Sci. Technol.*, *44*(10), 861–871, doi:10.1080/02786826.2010.498715.
Nguyen, T. K. V., M. D. Petters, S. R. Suda, H. Guo, R. J. Weber, and A. G. Carlton (2014), Trends in particle-phase liquid water during the Southern Oxidant and Aerosol Study, *Atmos. Chem. Phys.*, *14*(20), 10,911–10,930, doi:10.5194/acp-14-10911-2014.
O'Dowd, C. D., B. Langmann, S. Varghese, C. Scannell, D. Ceburnis, and M. C. Facchini (2008), A combined organic-inorganic sea-spray source function, *Geophys. Res. Lett.*, *35*, L01801, doi:10.1029/2007GL030331.
Ohmine, I., and T. Tanaka (1982), Salt effects on the phase transition of ionic gels, *J. Chem. Phys.*, *77*(11), 5725–5729, doi:10.1063/1.443780.
Orellana, M. V., P. A. Matrai, C. Leck, C. D. Rauschenberg, A. M. Lee, and E. Coz (2011), Marine microgels as a source of cloud condensation nuclei in the high Arctic, *Proc. Natl. Acad. Sci. U.S.A.*, *108*(33), 13,612–13,617, doi:10.1073/pnas.1102457108.
Ovadnevaite, J., D. Ceburnis, G. Martucci, J. Bialek, C. Monahan, M. Rinaldi, M. C. Facchini, H. Berresheim, D. R. Worsnop, and C. O'Dowd (2011), Primary marine organic aerosol: A dichotomy of low hygroscopicity and high CCN activity, *Geophys. Res. Lett.*, *38*, L21806, doi:10.1029/2011GL048869.
Petters, M. D., and S. M. Kreidenweis (2007), A single parameter representation of hygroscopic growth and cloud condensation nucleus activity, *Atmos. Chem. Phys.*, *7*, 1961–1971, doi:10.5194/acp-7-1961-2007.
Petters, M. D., and S. M. Kreidenweis (2008), A single parameter representation of hygroscopic growth and cloud condensation nucleus activity. Part 2: Including solubility, *Atmos. Chem. Phys.*, *8*(20), 6273–6279, doi:10.5194/acp-8-6273-2008.
Petters, M. D., and S. M. Kreidenweis (2013), A single parameter representation of hygroscopic growth and cloud condensation nucleus activity. Part 3: Including surfactant partitioning, *Atmos. Chem. Phys.*, *13*(2), 1081–1091, doi:10.5194/acp-13-1081-2013.
Petters, M. D., S. M. Kreidenweis, J. R. Snider, K. A. Koehler, Q. Wang, A. J. Prenni, and P. J. Demott (2006), Cloud droplet activation of polymerized organic aerosol, *Tellus, Ser. B*, *58*(3), 196–205, doi:10.1111/j.1600-0889.2006.00181.x.
Petters, M. D., A. J. Prenni, S. M. Kreidenweis, and P. J. DeMott (2007), On measuring the critical diameter of cloud condensation nuclei using mobility selected aerosol, *Aerosol Sci. Technol.*, *41*(10), 907–913, doi:10.1080/02786820701557214.
Petters, M. D., C. M. Carrico, S. M. Kreidenweis, A. J. Prenni, P. J. DeMott, J. L. Collett, and H. Moosmüller (2009a), Cloud condensation nucleation activity of biomass burning aerosol, *J. Geophys. Res.*, *114*, D22205, doi:10.1029/2009JD012353.

Petters, M. D., S. M. Kreidenweis, A. J. Prenni, R. C. Sullivan, C. M. Carrico, K. A. Koehler, and P. J. Ziemann (2009b), Role of molecular size in cloud droplet activation, *Geophys. Res. Lett.*, *36*, L22801, doi:10.1029/2009GL040131.

Petters, S. S., and M. D. Petters (2016), Surfactant effect on cloud condensation nuclei for two-component internally mixed aerosols, *J. Geophys. Res. Atmos.*, *121*, 1878–1895, doi:10.1002/2015JD024090.

Pöschl, U., et al. (2010), Rainforest aerosols as biogenic nuclei of clouds and precipitation in the Amazon, *Science*, *329*(5998), 1513–1516, doi:10.1126/science.1191056.

Prather, K. A., et al. (2013), Bringing the ocean into the laboratory to probe the chemical complexity of sea spray aerosol, *Proc. Natl. Acad. Sci. U.S.A.*, *110*(19), 7550–7555, doi:10.1073/pnas.1300262110.

Prenni, A. J., M. D. Petters, S. M. Kreidenweis, P. J. DeMott, and P. J. Ziemann (2007), Cloud droplet activation of secondary organic aerosol, *J. Geophys. Res.*, *112*, D10223, doi:10.1029/2006JD007963.

Raatikainen, T., and A. Laaksonen (2011), A simplified treatment of surfactant effects on cloud drop activation, *Geosci. Model Dev.*, *4*(1), 107–116, doi:10.5194/gmd-4-107-2011.

Raymond, T. M., and S. N. Pandis (2002), Cloud activation of single-component organic aerosol particles, *J. Geophys. Res.*, *107*(24), 4787, doi:10.1029/2002JD002159.

Raymond, T. M., and S. N. Pandis (2003), Formation of cloud droplets by multicomponent organic particles, *J. Geophys. Res.*, *108*(D15), 4469, doi:10.1029/2003JD003503.

Renbaum-Wolff, L., J. W. Grayson, A. P. Bateman, M. Kuwata, M. Sellier, B. J. Murray, J. E. Shilling, S. T. Martin, and A. K. Bertram (2013), Viscosity of secondary organic material and implications for particle growth and reactivity, *Proc. Natl. Acad. Sci. U.S.A.*, *110*(20), 8014–8019, doi:10.1073/pnas.1219548110.

Roberts, G. C., and A. Nenes (2005), A continuous-flow streamwise thermal-gradient CCN chamber for atmospheric measurements, *Aerosol Sci. Technol.*, *39*(3), 206–221, doi:10.1080/027868290913988.

Rosalam, S., and R. England (2006), Review of xanthan gum production from unmodified starches by Xanthomonas comprestris sp, *Enzyme Microb. Technol.*, *39*(2), 197–207, doi:10.1016/j.enzmictec.2005.10.019.

Rose, D., S. S. Gunthe, E. Mikhailov, G. P. Frank, U. Dusek, M. O. Andreae, and U. Pöschl (2008), Calibration and measurement uncertainties of a continuous-flow cloud condensation nuclei counter (DMT-CCNC): CCN activation of ammonium sulfate and sodium chloride aerosol particles in theory and experiment, *Atmos. Chem. Phys.*, *8*(5), 1153–1179, doi:10.5194/acp-8-1153-2008.

Russell, L. M., L. N. Hawkins, A. A. Frossard, P. K. Quinn, and T. S. Bates (2010), Carbohydrate-like composition of submicron atmospheric particles and their production from ocean bubble bursting, *Proc. Natl. Acad. Sci. U.S.A.*, *107*(15), 6652–6657, doi:10.1073/pnas.0908905107.

Sjogren, S., M. Gysel, E. Weingartner, U. Baltensperger, M. J. Cubison, H. Coe, A. A. Zardini, C. Marcolli, U. K. Krieger, and T. Peter (2007), Hygroscopic growth and water uptake kinetics of two-phase aerosol particles consisting of ammonium sulfate, adipic and humic acid mixtures, *J. Aerosol Sci.*, *38*(2), 157–171, doi:10.1016/j.jaerosci.2006.11.005.

Snider, J. R., and M. D. Petters (2008), Optical particle counter measurement of marine aerosol hygroscopic growth, *Atmos. Chem. Phys.*, *8*(7), 1949–1962, doi:10.5194/acp-8-1949-2008.

Sorjamaa, R., B. Svenningsson, T. Raatikainen, S. Henning, M. Bilde, and A. Laaksonen (2004), The role of surfactants in Köhler theory reconsidered, *Atmos. Chem. Phys.*, *4*(8), 2107–2117, doi:10.5194/acp-4-2107-2004.

Stokes, R., and R. Robinson (1966), Interactions in aqueous nonelectrolyte solutions. I. Solute-solvent equilibria, *J. Phys. Chem.*, *70*(7), 2126–2131, doi:10.1021/j100879a010.

Suda, S. R., and M. D. Petters (2013), Accurate determination of aerosol activity coefficients at relative humidities up to 99% using the Hygroscopicity Tandem Differential Mobility Analyzer technique, *Aerosol Sci. Technol.*, *47*(9), 991–1000, doi:10.1080/02786826.2013.807906.

Suda, S. R., M. D. Petters, A. Matsunaga, R. C. Sullivan, P. J. Ziemann, and S. M. Kreidenweis (2012), Hygroscopicity frequency distributions of secondary organic aerosols, *J. Geophys. Res.*, *117*, D04207, doi:10.1029/2011JD016823.

Suda, S. R., et al. (2014), Influence of functional groups on organic aerosol cloud condensation nucleus activity, *Environ. Sci. Technol.*, *48*(17), 10,182–10,190, doi:10.1021/es502147y.

Sullivan, R. C., M. J. K. Moore, M. D. Petters, S. M. Kreidenweis, G. C. Roberts, and K. A. Prather (2009), Effect of chemical mixing state on the hygroscopicity and cloud nucleation properties of calcium mineral dust particles, *Atmos. Chem. Phys.*, *9*(10), 3303–3316, doi:10.5194/acp-9-3303-2009.

Tanaka, M., T. Hayashi, and S. Morita (2013), The roles of water molecules at the biointerface of medical polymers, *Polym. J.*, *45*(7), 701–710, doi:10.1038/pj.2012.229.

Torres, M. D., R. Moreira, F. Chenlo, and M. J. Vázquez (2012), Water adsorption isotherms of carboxymethyl cellulose, guar, locust bean, tragacanth and xanthan gums, *Carbohydr. Polym.*, *89*(2), 592–598, doi:10.1016/j.carbpol.2012.03.055.

Verdugo, P. (2012), Marine microgels, *Annu. Rev. Mar. Sci.*, *4*(1), 375–400, doi:10.1146/annurev-marine-120709-142759.

Virkkula, A., R. Van Dingenen, F. Raes, and J. Hjorth (1999), Hygroscopic properties of aerosol formed by oxidation of limonene, α-pinene, and β-pinene, *J. Geophys. Res.*, *104*(D3), 3569–3579, doi:10.1029/1998JD100017.

Wang, S. C., and R. C. Flagan (1990), Scanning electrical mobility spectrometer, *Aerosol Sci. Technol.*, *13*(2), 230–240, doi:10.1080/02786829008959441.

Wexler, A. S., and S. L. Clegg (2002), Atmospheric aerosol models for systems including the ions H^+, NH_4^+, Na^+, SO_4^{2-}, NO_3^-, Cl^-, Br^-, and H_2O, *J. Geophys. Res.*, *107*(D14), 4207, doi:10.1029/2001JD000451.

Wisniewski, S., and S. W. Kim (1980), Permeation of water through poly(2-hydroxyethyl methacrylate) and related polymers: Temperature effects, *J. Membr. Sci.*, *6*, 309–318, doi:10.1016/S0376-7388(00)82172-9.

Wyatt, N. B., and M. W. Liberatore (2009), Rheology and viscosity scaling of the polyelectrolyte xanthan gum, *J. Appl. Polym. Sci.*, *114*(6), 4076–4084, doi:10.1002/app.31093.

Yoshida, H., T. Hatakeyama, and H. Hatakeyama (1992), Effect of water on the main chain motion of polysaccharide hydrogels, in *Viscoelasticity of Biomaterials*, vol. 489, edited by W. Glasser and H. Hatakeyama, *ACS Symp. Ser.*, pp. 217–230 , Am. Chem. Soc., Washington, D. C.

Yoshida, T., M. Takahashi, T. Hatakeyama, and H. Hatakeyama (1998), Annealing induced gelation of xanthan/water systems, *Polymer (Guildf)*, *39*(5), 1119–1122, doi:10.1016/S0032-3861(97)00266-8.

Zardini, A. A., S. Sjogren, C. Marcolli, U. K. Krieger, M. Gysel, E. Weingartner, U. Baltensperger, and T. Peter (2008), A combined particle trap/HTDMA hygroscopicity study of mixed inorganic/organic aerosol particles, *Atmos. Chem. Phys.*, *8*(18), 5589–5601, doi:10.5194/acp-8-5589-200.

Zdanovskii, A. B. (1948), New methods for calculating solubilities of electrolytes in multicomponent systems, *Zh. Fiz. Khim.*, *22*, 1475–1485.

Zhang, Y., et al. (2015), Changing shapes and implied viscosities of suspended submicron particles, *Atmos. Chem. Phys.*, *15*(14), 7819–7829, doi:10.5194/acp-15-7819-2015.

Zuend, A., C. Marcolli, B. P. Luo, and T. Peter (2008), A thermodynamic model of mixed organic-inorganic aerosols to predict activity coefficients, *Atmos. Chem. Phys.*, *8*(16), 4559–4593, doi:10.5194/acp-8-4559-2008.

Zuend, A., C. Marcolli, A. M. Booth, D. M. Lienhard, V. Soonsin, U. K. Krieger, D. O. Topping, G. McFiggans, T. Peter, and J. H. Seinfeld (2011), New and extended parameterization of the thermodynamic model AIOMFAC: Calculation of activity coefficients for organic-inorganic mixtures containing carboxyl, hydroxyl, carbonyl, ether, ester, alkenyl, alkyl, and aromatic functional groups, *Atmos. Chem. Phys.*, *11*(17), 9155–9206, doi:10.5194/acp-11-9155-2011.